Fast blood flow simulations in three-dimensional arterial trees.

L. A. Mansilla Alvarez

P. J. Blanco

R. A. Feijóo

lalvarez@lncc.br

pjblanco@lncc.br

feij@lncc.br

National Laboratory for Scientific Computing, LNCC/MCTIC, Av. Getúlio Vargas 333, 26561-075, Petrópolis, Brazil.

National Institute of Science and Technology in Medicine Assisted by Scientific Computing, INCT-MACC, Petrópolis, Brazil.

Abstract. *Even when computational techniques, aiming to simulate the blood flow through the cardiovascular system, can provide valuable information to study the onset and localization of diseases such as atherosclerosis, their massive use in the daily medical practice has been strongly limited by the enormous computational burden (in terms of simulation time and physical resources) implied by these methodologies. Simulation time in the order of days, or even with the use of hundreds of processors, are prohibitive in medical practice. In this work, we explore a novel methodology capable to provide detailed spatial information of the blood flow dynamic with a severe reduction in the computational cost in comparison with standard 3D FEM simulations. This methodology, called Transversally Enriched Pipe Element Method (TEPEM), exploits geometrical characteristics of the regions of interest, as well as hemodynamics phenomena a priori known, to propose a pipe-tailored discretization of the Navier-Stokes equations. This approach is capable to efficiently approximate the 3D dynamics of physical fields exhibiting a considerable cost reduction. The TEPEM advantages are studied through numerical examples in geometries obtained via image segmentation of patient-specific arterial regions.*

Keywords: *Hemodynamics, TEPEM, Model order reduction, Finite element method, Patient-specific*

1 INTRODUCTION

In cardiovascular research, an accurate description of flow-related quantities via computational modeling is a fundamental tool to study the onset and localization of several diseases (Taylor et al., 2013). Many authors have correlated the initiation of cardiovascular diseases with perturbations in the blood stream, by studying the velocity profile, spatial pressure distribution or wall shear stress (WSS) on specific regions of the circulatory system (Fox and Hugh, 1966; Zarins et al., 1983; Ku et al., 1985; Giannoglou et al., 2002). This evidence motivated the development of several techniques to combine medical image processing and numerical simulation of the blood flow in order to provide an efficient and non-invasive strategy to aid in the prognosis and diagnosis of diseases such as atherosclerosis, while taking in consideration the particularities of each patient-specific geometry.

Regarding current numerical methodologies, these can be roughly divided into two groups: by-element methods, such as finite element/volume techniques (Perktold et al., 1991; Taylor et al., 1998), and reducer-order approaches, as the proper orthogonal decomposition or reduced basis method (Lucia et al., 2004; Quarteroni and Rozza, 2014), just to mention the two more popular choices. While by-element methods provide accurate results by discretizing the domain into several small elements, the reduced-order approaches search for the approximate solution into a finite-dimensional space spanned by a priori computed basis functions, obtained according to some characteristics of the problem.

Notwithstanding the high degree of accuracy that can be obtained with these numerical methodologies, the computational effort demanded in these simulations is often excessive and prohibitive in the daily medical practice (Grinberg et al., 2009). Furthermore, even for a detailed description of the hemodynamic indexes such as WSS or the oscillatory shear index (OSI), a high degree of precision provided by high-fidelity methods is often overreaching the practical needs. Large-scale simulations employing the Finite Element Method (FEM), based on tetrahedral meshes, can achieve computational time in the order of days for a single cardiac cycle. Reducer-order approaches reduce the time of these simulations in detriment of an *offline-step* to compute the basis functions of the finite dimensional space in where the approximation is sought. This offline step demands an enormous computational effort sometimes beyond the total cost of FEM.

To deal with the high computational effort, in terms of simulation time and physical resources required, dimensionally reduced models are employed to obtain a global knowledge on the dynamic but now in a time in the order of minutes. One-dimensional models, obtained considering kinematical hypotheses, are one of the most popular choices due the capability to provide an accurate approximation on the pressure drop and wave propagation in large-scale simulations with an extreme reduction in the computational cost in comparison to full 3D methods (Blanco et al., 2014; Grinberg et al., 2011; Hughes and Lubliner, 1973). However, the very kinematical hypotheses that help in the reduction of the problem made it unsuitable to predict the heterogeneous structure of the blood flow, which is a fundamental aspect for the accurate estimation of WSS over the endothelium in complex patient-specific geometries.

In (Blanco et al., 2015; Mansilla Alvarez et al., 2017), the authors proposed a numerical alternative to deal with the trade-off between accuracy and efficiency presented in current methodologies. The approach, coined as Transversally Enriched Pipe Element Method (TEPEM), is especially aimed for the use in hemodynamics by exploiting some very important

characteristics in the cardiovascular system: the pipe-like structure of the domain of interest and the dominantly axial dynamics of the blood flow. Coupling a slab-type partition of the computational domain and an interpolation with different polynomial functions, whose order depends on the flow direction, the TEPEM provides an efficient alternative to approximate blood flow dynamics with enough accuracy for medical practice while featuring a severe reduction in the computational effort when compared with standard FEM simulations.

In this work, we explore the predictive capabilities of TEPEM in branching domains aiming at its application in hemodynamic studies performed in large patient-specific arterial trees. For this, a meshing strategy based on pipe-elements and the adaptation of field interpolants to accurately deal with bifurcated regions, where complex blood patterns develop, is proposed with versatility enough to be extended to patient-specific geometries.

The document is organized as follows. Section 2 describes the fluid flow problem. In Section 3 the meshing strategy is presented, which is based in pipe-like elements, for an arbitrary branching domain. Construction of interpolants for the TEPEM is in Section 4. Numerical results are reported and discussed in Section 5 and final remarks are drawn in Section 6.

2 MODEL PROBLEM

Let $\Omega \subset \mathbb{R}^3$ with boundary $\Gamma = \Gamma_i \cup \Gamma_o \cup \Gamma_L$, being Γ_i and Γ_o the inlet and outlet boundaries, respectively. Lateral boundary (the arterial wall) is considered smooth and denoted by Γ_L. Figure 1 presents a geometrical description of the domain of analysis for the fluid flow problem. In this domain, the inlet and outlet boundaries are considered to be flat.

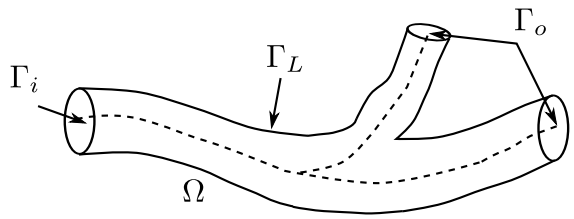

Figure 1: Geometrical description of a typical domain in blood flow simulations.

At inlet and outlet boundaries, conditions of Neumann or Dirichlet type are prescribed. Defective boundary conditions, as for example the prescription of flow rate, are also possible to be imposed through Lagrange multipliers. Once we are interested in simulating the blood flow into a domain corresponding to an isolated region of the cardiovascular system, it is valid to assume that the flow is fully developed at the entrance and exists of this region. This hypothesis implies in uniform normal component of the traction and null in-plane velocity components. Over the lateral boundary Γ_L no-slip boundary conditions are considered.

Then, the variational formulation for the fluid flow problem reads: find $(\mathbf{u}, p) \in \boldsymbol{\mathcal{V}} \times L^2(\Omega)$ such that

$$\begin{aligned} \int_\Omega \left[\rho \frac{\partial \mathbf{u}}{\partial t} \cdot \hat{\mathbf{u}} + \rho(\nabla \mathbf{u})\mathbf{u} \cdot \hat{\mathbf{u}} + 2\mu \boldsymbol{\varepsilon}(\mathbf{u}) \cdot \boldsymbol{\varepsilon}(\hat{\mathbf{u}}) - p \operatorname{div} \hat{\mathbf{u}} - \hat{p} \operatorname{div} \mathbf{u} \right] d\Omega = \\ \int_{\Gamma_i} t_i \mathbf{n} \cdot \hat{\mathbf{u}} \, d\Gamma_i + \int_{\Gamma_o} t_o \mathbf{n} \cdot \hat{\mathbf{u}} \, d\Gamma_o \qquad \forall (\hat{\mathbf{u}}, \hat{p}) \in \boldsymbol{\mathcal{V}} \times L^2(\Omega), \end{aligned} \tag{1}$$

with ρ and μ being the fluid density and viscosity, respectively, $\boldsymbol{\varepsilon}(\cdot) = (\nabla(\cdot))^S$, $\mathbf{n}$ is the outward normal unit vector and $\hat{(\cdot)}$ denotes an admissible variation of field $(\cdot)$. Space $\boldsymbol{\mathcal{V}}$ is

$$\boldsymbol{\mathcal{V}} = \{\mathbf{u} \in \mathbf{H}^1(\Omega); \mathbf{u}|_{\Gamma_L} = \mathbf{0},\ (\boldsymbol{\Pi}\mathbf{u})|_{\Gamma_i} = \mathbf{0},\ (\boldsymbol{\Pi}\mathbf{u})|_{\Gamma_o} = \mathbf{0}\}, \tag{2}$$

with $\mathbf{H}^1(\Omega) = [H^1(\Omega)]^3$, and where $\boldsymbol{\Pi} = \mathbf{I} - \mathbf{n} \otimes \mathbf{n}$ is the projection operator over the surface whose normal unit vector is $\mathbf{n}$. Finally, t_i and t_o are given data which stand for the magnitude of the normal component of the traction vector imposed at Γ_i and Γ_o, respectively.

3 TEPEM MESH: PIPE ELEMENT DISCRETIZATION

The first ingredient in the TEPEM approach is the meshing strategy to discretize the computational domain. Once our main interest is to model the blood flow into arterial trees, we can consider each domain of analysis as a network of tubular regions. The special tubular structure of the domain allows us to define a geometrical discretization based in tubular finite elements as described next. These finite elements are referred to as *pipe elements* and are composed by slices of the arterial vessel in the axial direction.

To explain the mesh characteristics, let us explore two particular cases. First, the case in which the arterial region is a simple non-branching domain. The second case will explore the geometric mesh for branching domains.

3.1 Tubular domains

For simple tubular regions, without bifurcations, a natural subdivision into slab elements is performed transversally slicing the domain following the axial direction of the pipe. The domain, denoted by Ω, is then discretized into a slab-type partition $\mathcal{T}_h(\Omega)$ parametrized by the mesh parameter h associated to the axial length of the elements. Any pipe element $\mathcal{K} \in \mathcal{T}_h(\Omega)$ is mapped into the reference element $\mathcal{K}_0 = [-1, 1]^3$ (in the space $\xi\eta\zeta$), through a mapping denoted by $\chi_\mathcal{K}$, and maintaining the axial direction aligned with the ζ-axis. A geometrical description of the mesh structure is presented in Figure 2.

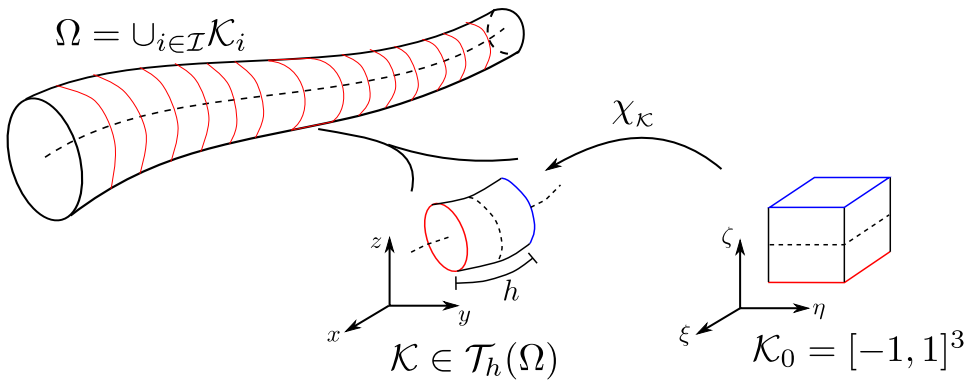

Figure 2: Geometrical mesh formed by pipe-elements for a non-branching domain Ω.

The geometrical mapping between the reference element $\mathcal{K}_0$ and any pipe element $\mathcal{K}$ is defined as follows

$$\chi_\mathcal{K}(\xi, \eta, \zeta) = \sum_{k=1}^{3}\sum_{n=1}^{12} \mathbf{x}_n^k \mathcal{S}_n(\xi, \eta) Q_k(\zeta), \qquad (\xi, \eta, \zeta) \in \mathcal{K}_0 = [-1, 1]^3 \tag{3}$$

where $\{Q_i, i = 1, 2, 3\}$ stand by the classical Lagrangian basis for the space of quadratic polynomials $\mathbb{P}_2$ and the set $\{\mathcal{S}_n, n = 1, \ldots, 12\}$ is the 2 D cubic Serendipity basis defined as:

$$
\begin{aligned}
\mathcal{S}_1(\xi,\eta) &= \frac{1}{32}(1+\xi)(1-\eta)(9(\xi^2+\eta^2)-10) & \mathcal{S}_7(\xi,\eta) &= \frac{9}{32}(1-\xi^2)(1+3\xi)(1+\eta)\\
\mathcal{S}_2(\xi,\eta) &= \frac{1}{32}(1+\xi)(1+\eta)(9(\xi^2+\eta^2)-10) & \mathcal{S}_8(\xi,\eta) &= \frac{9}{32}(1-\xi^2)(1-3\xi)(1+\eta)\\
\mathcal{S}_3(\xi,\eta) &= \frac{1}{32}(1-\xi)(1+\eta)(9(\xi^2+\eta^2)-10) & \mathcal{S}_9(\xi,\eta) &= \frac{9}{32}(1-\xi)(1-\eta^2)(1+3\eta)\\
\mathcal{S}_4(\xi,\eta) &= \frac{1}{32}(1-\xi)(1-\eta)(9(\xi^2+\eta^2)-10) & \mathcal{S}_{10}(\xi,\eta) &= \frac{9}{32}(1-\xi)(1-\eta^2)(1-3\eta)\\
\mathcal{S}_5(\xi,\eta) &= \frac{9}{32}(1+\xi)(1-\eta^2)(1-3\eta) & \mathcal{S}_{11}(\xi,\eta) &= \frac{9}{32}(1-\xi^2)(1-3\xi)(1-\eta)\\
\mathcal{S}_6(\xi,\eta) &= \frac{9}{32}(1+\xi)(1-\eta^2)(1+3\eta) & \mathcal{S}_{12}(\xi,\eta) &= \frac{9}{32}(1-\xi^2)(1+3\xi)(1-\eta)
\end{aligned}
\tag{4}
$$

In the same mapping, $\{\mathbf{x}_n^k, n = 1, \ldots, 12\}$ is a set of points on the transversal section mapped from the section $\zeta = k - 2$ in the reference element. This strategy allows us to approximate any cross-section with enough degree of accuracy as neededed from a practical point of view for the field in where the methodology is to be applied.

3.2 Branching domains

For a case of a simple branching vessel, the discretization is an extension of the strategy described for simple tubular regions. Let us consider Ω as a simple branching domain. To perform a slab-type partition, lets first divide Ω by dividing the three non-bifurcated regions, denoted as Ω_i ($i = A, B, C$) as in Figure 3. The use of simple pipe-elements, as those described in the previous section, is enough to discretize these tubular regions but is insufficient for the discretization of the domain of the junction, denoted by ω in the same figure. For this reason we propose *special elements* to effectively refine the mesh in the transversal direction.

The *special element*, denoted by $\mathcal{K}_i^*$ ($i = A, B, C$) in panel (c) in Figure 3, appears as a pipe extension of the denominated transition element proposed by Gupta (1978) for the non-conforming mesh refinement of quadrilateral meshes, locally refining the mesh by coupling one single pipe element with two of them in the transversal direction. Employing this extension of simple pipe-elements, it is possible to define a domain partition, $\mathcal{T}_h(\Omega)$, based on pipe elements with a mesh refinement in the bifurcation region which also increases the predictive capabilities of the model by increasing the number of transversal elements instead of the transversal polynomial order for the interpolant basis.

Each of these special elements is composed by four planar sections related to $\zeta = -1$, $\zeta = 0$, $\{\zeta = 1, \eta < 0\}$ and $\{\zeta = 1, \eta \geq 0\}$ in the reference element $\mathcal{K}_0$, as can be seen in panel (d) in Figure 3. Note that, in contrast with the non-branching case, one section in the reference element is cut in half to handle the branching nature of the special element. While each simple

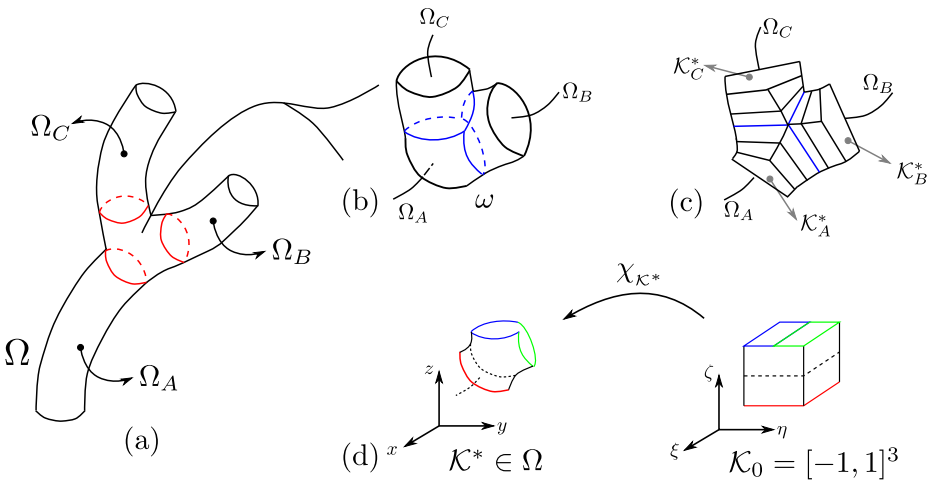

Figure 3: Geometrical mesh based in pipe-elements for a non-branching domain Ω.

element $\mathcal{K} \in \mathcal{T}_h(\Omega)$ is related to the reference element $\mathcal{K}_0$ via the mapping (3), a generic special element $\mathcal{K}^*$ is mapped into $\mathcal{K}_0$ via the following transformation

$$\chi_{\mathcal{K}^*}(\xi,\eta,\zeta) = \sum_{k=1}^{4}\sum_{n=1}^{12} \mathbf{x}_n^k \hat{\mathcal{S}}_{nk}(\xi,\eta,\zeta) \tag{5}$$

where $\{\mathbf{x}_n^k, n = 1,\dots,12\}$ is a set of points on the transversal section mapped from the section $\zeta = -1$ $(k = 1)$, $\zeta = 0$ $(k = 2)$, $\{\zeta = 1, \eta < 0\}$ $(k = 3)$ and $\{\zeta = 1, \eta \geq 0\}$ $(k = 4)$ in the reference element, and the functions $\hat{\mathcal{S}}_{nk}$ are defined as:

$$\begin{aligned}
\hat{\mathcal{S}}_{nk}(\xi,\eta,\zeta) &= \mathcal{S}_n(\xi,\eta)Q_k(\zeta) && k = 1,2;\ n = 1,\dots,12,\\
\hat{\mathcal{S}}_{n3}(\xi,\eta,\zeta) &= \mathcal{S}_n(\xi,2\eta+1)Q_3(\zeta) && n = 1,\dots,12,\\
\hat{\mathcal{S}}_{n4}(\xi,\eta,\zeta) &= \mathcal{S}_n(\xi,2\eta-1)Q_3(\zeta) && n = 1,\dots,12.
\end{aligned} \tag{6}$$

The geometrical algorithm here presented can be straightforwardly extended to include domains with several bifurcations or even with more complex junctions, providing a generic and computationally cheap meshing strategy when compared with tetrahedral mesh generation algorithms.

4 TEPEM INTERPOLANTS: TRANSVERSAL ENRICHMENT

Regarding to the interpolation strategy in the TEPEM approach, this is constructed resorting to the fact that the blood flow is dominantly axial throughout the cardiovascular system. Based on this *a priori* knowledge, we proposed to differentiate the degree of polynomial approximation given to axial and transversal directions for any field, in the reference element $\mathcal{K}_0$.

That is, for a defined slab-type partition $\mathcal{T}_h(\Omega)$, we approximate any scalar field w by the function w^h in the finite-dimensional space

$$\mathbb{T}_h^{\mathsf{p},\mathsf{s}} = \left\{ w^h \in L^2(\Omega) : w^h \circ \chi_{\mathcal{K}}(\xi,\eta,\zeta) = \sum_{j=1}^{\mathsf{s}+1} w_j^{\mathsf{p}}(\xi,\eta)\varphi_j(\zeta), \quad \mathcal{K} \in \mathcal{T}_h(\Omega) \right\} \tag{7}$$

where $\{\varphi_j : j = 1, \ldots, \mathsf{s}+1\}$ is a basis for the space $\mathbb{P}_\mathsf{s}$ of polynomials up to degree s defined in $\zeta \in [-1, 1]$, and the functions $\{w_j^\mathsf{p} : j = 1, \ldots, \mathsf{s}+1\}$ are defined according to the type of element $\mathcal{K} \in \mathcal{T}_h(\Omega)$. For a simple element, the functions w_j^p are defined by

$$w_j^\mathsf{p}(\xi, \eta) = \sum_{i=1}^{(\mathsf{p}+1)^2} w_{ij}^h \phi_i(\xi, \eta) \qquad j = 1, \ldots, \mathsf{s}+1, \tag{8}$$

while for a transition element, they have the form

$$w_j^\mathsf{p}(\xi, \eta) = \begin{cases} \displaystyle\sum_{i=1}^{(\mathsf{p}+1)^2} w_{ij}^h \phi_i(\xi, \eta) & j \leq \mathsf{s}, \\ \displaystyle\sum_{i=1}^{(\mathsf{p}+1)^2} \hat{w}_{ij}^h \phi_i(\xi, 2\eta+1)\mathbb{1}_{\eta<0} + \check{w}_{ij}^h \phi_i(\xi, 2\eta-1)\mathbb{1}_{\eta\geq 0} & j = \mathsf{s}+1, \end{cases} \tag{9}$$

with $\{\phi_i : i = 1, \ldots, (\mathsf{p}+1)^2\}$ a basis for the two-dimensional space $\mathbb{P}_\mathsf{p} \times \mathbb{P}_\mathsf{p}$, being $\xi \times \eta \in [-1, 1] \times [-1, 1]$, and $\mathbb{1}_{\eta<0}$ ($\mathbb{1}_{\eta\geq 0}$) the characteristic function of the set defined for $\eta < 0$ ($\eta \geq 0$).

Axial dependence of the field w, aligned with the axis ζ in the reference element, is approximated through polynomial functions up to order s (axial order) while transversal dependence is approximated by polynomials up to order p (transversal order). The particular case when $\mathsf{s} = \mathsf{p}$ can be understood as a variant of classical pFEM assembled on top of a very specific pipe-element partition.

Our main assumption is that, given a low axial order s, the transversal dynamics can be accurately approximated by employing polynomials of order in the range $4 \leq \mathsf{p} \leq 10$. This allows us to substantially reduce the computational complexity of the problem maintaining reasonably good predictive capabilities. This hypothesis has been conferred in non-branching patient-specific regions, where accurate approximation in the wall shear stress is computed with an estimated gain in computational time ranging between 150 and 600 for transient simulations.

Once a partition $\mathcal{T}_h(\Omega)$ of $\Omega \subset \mathbb{R}^3$ has been defined, and for a transversal order defined by an even parameter $\mathsf{p} \in \mathbb{N}$, we introduce the finite-dimensional spaces for the velocity and pressure fields

$$\boldsymbol{\mathcal{V}}_h = \left[\mathbb{T}_h^{\mathsf{p},2}\right]^3 \cap C(\overline{\Omega}) \cap \boldsymbol{\mathcal{V}} \qquad \mathcal{Q}_h = \mathbb{T}_h^{\frac{\mathsf{p}}{2},1}. \tag{10}$$

This is, we consider the approximate velocity as being a continuous field, while the pressure is regarded as a discontinuous field. The semi-discrete variational problem becomes: Find $(\mathbf{u}^h, p^h) \in \boldsymbol{\mathcal{V}}_h \times \mathcal{Q}_h$ such that

$$\begin{aligned} \int_\Omega \left[\rho \frac{\partial \mathbf{u}^h}{\partial t} \cdot \hat{\mathbf{u}}^h + \rho(\nabla \mathbf{u}^h)\mathbf{u}^h \cdot \hat{\mathbf{u}}^h + 2\mu\boldsymbol{\varepsilon}(\mathbf{u}^h) \cdot \boldsymbol{\varepsilon}(\hat{\mathbf{u}}^h) - p^h \operatorname{div} \hat{\mathbf{u}}^h - \hat{p}^h \operatorname{div} \mathbf{u}^h\right] d\Omega = \\ \int_{\Gamma_i} t_i \mathbf{n} \cdot \hat{\mathbf{u}}^h \, d\Gamma_i + \int_{\Gamma_o} t_o \mathbf{n} \cdot \hat{\mathbf{u}}^h \, d\Gamma_o \qquad \forall (\hat{\mathbf{u}}^h, \hat{p}^h) \in \boldsymbol{\mathcal{V}}_h \times \mathcal{Q}_h. \end{aligned} \tag{11}$$

A fully discrete scheme is further obtained by employing an implicit backward Euler scheme for the time discretization and by Picard iterations to linearize the convective term. Regarding the field interpolants, a basis for each discrete space in (10) must be declared. For axial

interpolation, classical Lagrangian basis for $\mathbb{P}_2$ is considered for the velocity field while linear Lagrangian basis is considered for pressure. For the transverse polynomials, the product of two one-dimensional Lagrange polynomials is considered, defined in the coordinates ξ and η. Each function $\phi_i \in \mathbb{P}_\mathsf{p} \times \mathbb{P}_\mathsf{p}$ is defined by

$$\phi_i(\xi,\eta) = \hat{\phi}_j(\xi)\hat{\phi}_k(\eta) \qquad (\xi,\eta) \in [-1,1]^2 \tag{12}$$

where the indexes i and (j,k) are related through a bijection between the set $\{1,\ldots,(\mathsf{p}+1)^2\}$ and $\{1,\ldots,\mathsf{p}+1\}\times\{1,\ldots,\mathsf{p}+1\}$. Furthermore, the set $\{\hat{\phi}_i, i=1,\ldots,\mathsf{p}+1\}$ stands for the Lagrange basis functions defined in the set of Chebyshev-Gauss-Lobatto (CGL) nodes, this is, each $\hat{\phi}_i$ is given by

$$\hat{\phi}_i(\xi) = \prod_{n=1,n\neq i}^{\mathsf{p}+1} \frac{\xi - x_n}{x_i - x_n} \qquad i = 1,\ldots,\mathsf{p}+1 \tag{13}$$

where the set $\{x_n : n = 1,\ldots,\mathsf{p}+1\}$ is defined by

$$x_n = -\cos\left(\frac{\pi(n-1)}{\mathsf{p}}\right) \qquad n = 1,\ldots,\mathsf{p}+1 \tag{14}$$

These points are preferred over the ntural choice of equi-distant distribution of nodes, due to their properties to control the oscillating behavior of high-order interpolants. This problem in the interpolation by high-order polynomials, referred as *Runge phenomenon*, is graphically presented in Figure 4 as well as a comparison of the interpolated function employing the proposed set of CGL nodes.

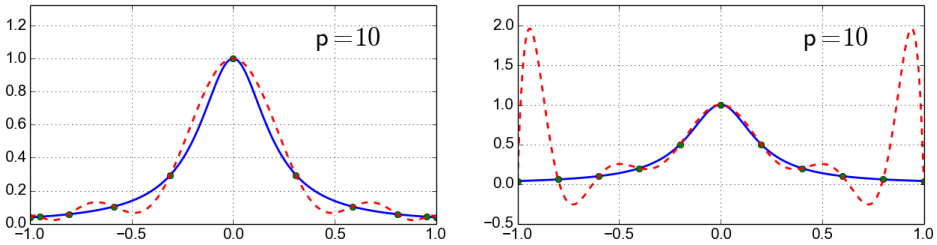

Figure 4: Runge phenomenom: Interpolation of Runge function $f(x) = (1+25x^2)^{-1}$ employing CGL nodes (left) and equispaced nodes (right).

5 NUMERICAL ASSESSMENT

In order to demonstrate the capabilities of the TEPEM in the hemodynamic field, in this section the methodology is tested in a synthetic bifurcated domain and in a patient-specific left coronary tree. The TEPEM solution is compared, quantitatively and quantitatively, to a reference solution obtained via standard FEM approximation. The FEM approach is based on the mini element in which the bubble degrees of freedom are consistently condensed and computed, and spurious oscillations caused by dominating convective terms are eliminated using SUPG stabilization. In both examples, blood properties are set to $\rho = 1.04\,\mathrm{g/cm^3}$ and $\mu = 0.04\,\mathrm{P}$. The system of algebraic equations is solved monolithically using a direct parallel algebraic LU solver for the TEPEM and an iterative GMRES method for the FEM. In Figure 5, we present both geometries employed for the numerical simulations.

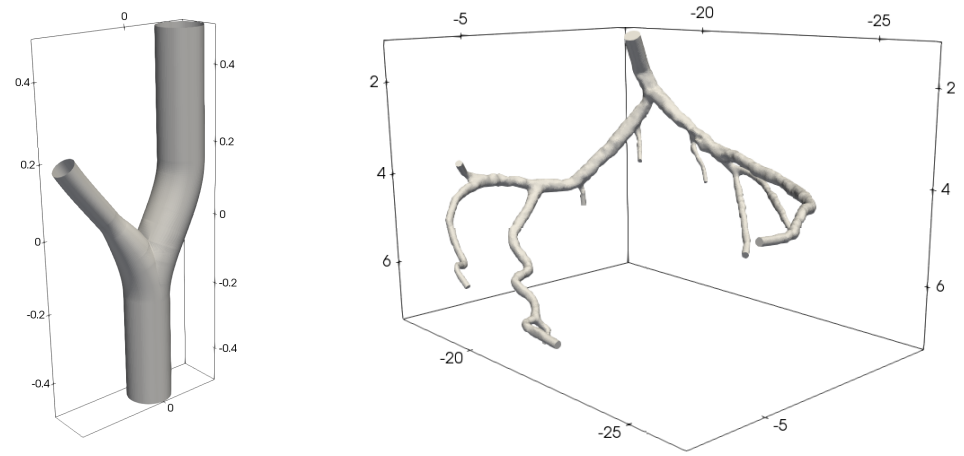

Figure 5: Geometries for the numerical experiments. Left: Synthetic bifurcation. Right: Patient-specific left coronary tree.

5.1 Simple synthetic bifurcation

In the first example, we consider the steady flow of a fluid, in a simple bifurcated domain, characterized by a Reynolds number equal to $\mathrm{Re} = 250$. This example is devoted to studying accuracy properties and convergence with respect to a reference solution obtained via standard FEM in a extremely fine tetrahedral mesh. In addition of TEPEM simulations, we also consider FEM simulations in coarser meshes to study the convergence also of this methodology. The characteristics of the meshes for both approaches are summarized in Table 1, as well as the error (measured in the $L^2(\Omega)$ norm) for velocity and pressure obtained with TEPEM and FEM compared against the reference solution.

Regarding to the reference solution, that approximation is obtained considering a tetrahedral mesh composed by $5\,631\,877$ elements and $4\,903\,064$ degrees of freedom. Assuming a linear parallel scalability and employing the same quantity of processors that were used for TEPEM simulations, this reference solution took approximately 600 minutes. This reflects a gain in the computational time ranging between 2000 and 250 times for $\mathsf{p} = 4$ and $\mathsf{p} = 8$.

In order to better understand the predictive capabilities of the TEPEM, in Figure 6 is presented the convergence behavior of TEPEM as a function of the transversal order p and the degrees of freedom. Still in the same figure, and to compare the TEPEM approach with classical FEM approximations, it is also presented the convergence behavior of FEM in function of characteristic element size h and the degrees of freedom.

Furthermore, in Figures 7 - 9 we present the velocity and pressure approximation for different transversal order in the TEPEM, and the comparison with the reference FEM solution. These figures provide a quantitative information on the TEPEM predictive capabilities, that is the capacity to accurately approximate velocity and pressure fields even for low transversal order and, particularly, at the bifurcated region where the blood flow features a more complex structure in comparison with tubular regions in the computational domain. It is also worth mentioning the potentialities of TEPEM to approximate the secondary flows, as can be seen in Figure 8.

Table 1: Comparison of computational effort and accuracy for the TEPEM and FEM. All the cases for TEPEM and FEM are simulated using the same number of computational nodes. For the accuracy study, both methodologies are compared against a FEM solution with a total of $4\,903\,064$ degrees of freedom and $5\,631\,877$ elements.

		Computational effort			Error	
Method		Elements	DoFs	Time (min)	$\|v - v_h\|^2$	$\|p - p_h\|^2$
TEPEM	$\mathsf{p} = 4$	220	34 360	0.3	0.074243	116.27901
	$\mathsf{p} = 6$	220	68 266	2.4	0.029104	44.813802
	$\mathsf{p} = 8$	220	113 718	10.5	0.005007	18.730026
	$\mathsf{p} = 10$	220	170 716	36.1	0.003179	12.055404
	$\mathsf{p} = 12$	220	239 260	114.2	0.002485	6.2524727
FEM	$h = 0.012$	198 348	137 844	3.5	0.104832	112.57084
	$h = 0.01$	344 690	235 480	9.8	0.046576	60.573951
	$h = 0.008$	676 435	454 336	36.2	0.016205	26.188051
	$h = 0.006$	1 626 317	1 072 612	148.4	0.003197	9.8464527

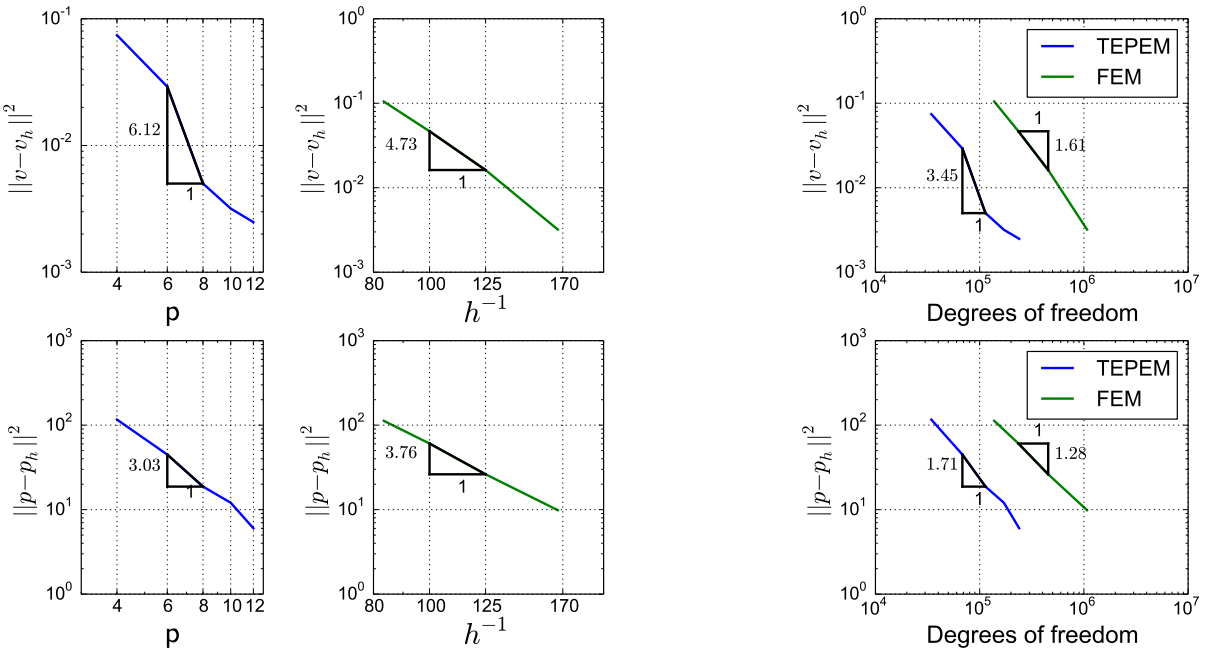

Figure 6: Numerical convergence of the velocity and pressure fields for the TEPEM and FEM compared with a reference FEM solution obtained with an extremely fine tetrahedral mesh. Also, the convergence of these fields as a function of the degrees of freedom is shown for both TEPEM and FEM.

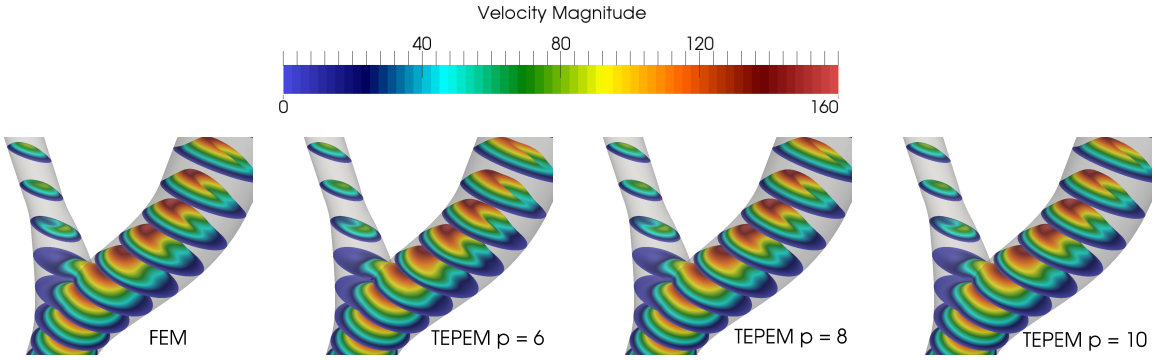

Figure 7: Velocity profiles at the bifurcation region with FEM and TEPEM using $\mathrm{p} = 6$**,** $\mathrm{p} = 8$ **and** $\mathrm{p} = 10$**.**

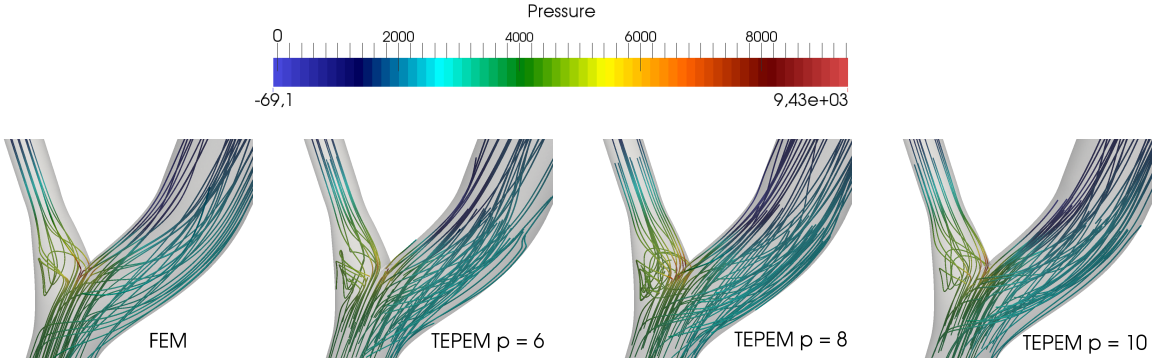

Figure 8: Streamlines for the velocity field at the bifurcation region with FEM and TEPEM using $\mathrm{p} = 6$**,** $\mathrm{p} = 8$ **and** $\mathrm{p} = 10$**. Color stands for the magnitude of pressure field.**

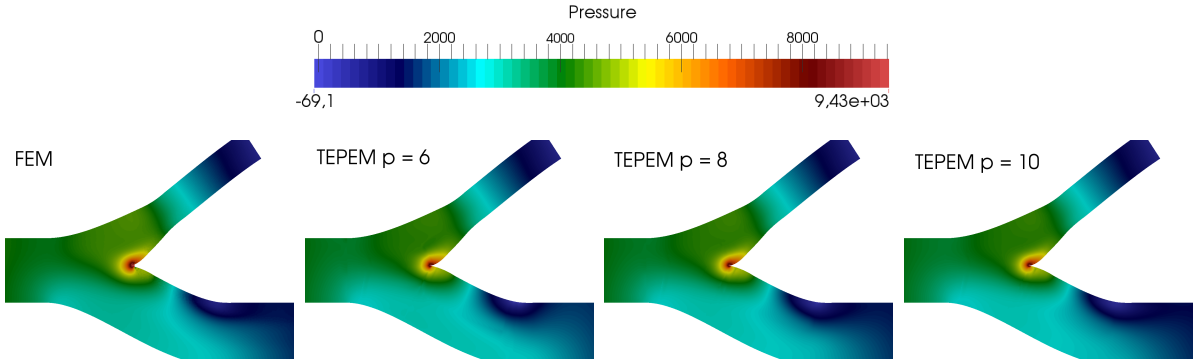

Figure 9: Pressure profile at the bifurcation region with FEM and TEPEM using $\mathrm{p} = 6$**,** $\mathrm{p} = 8$ **and** $\mathrm{p} = 10$**.**

5.2 Patient-specific coronary tree

This example is devoted to analyze the capabilities of the presented approach for the simulation of coronary blood flow in a patient-specific geometry of the left coronary tree obtained from computed tomography angiography. At the inlet, homogeneous Neumann condition is imposed. The flow rate is prescribed to be $Q = 2\mathrm{cm}^3/\mathrm{s}$, which is distributed among the outlet boundaries following a power law criterion in terms of vessel radii. The associated Reynolds number results Re = 150 when measured in the inlet section.

For comparison purposes, the reference FEM simulation is composed by $4\,094\,885$ tetra-

hedral elements, resulting in $2\,814\,015$ degrees of freedom and for which 50 processors (NP, number of processors) are required for its solution. In this case, a coarser FEM mesh is utilized, similar to that employed in simulations performed routinely. For the TEPEM, the pipe mesh is composed by 476 slab elements, while the number of degrees of freedom depends upon the transversal order. For the TEPEM solution, 10 NP are employed.

As way to perform a time comparison between TEPEM and FEM approximations, an average computational time is defined by multiplying the wall-clock simulation time and the NP employed in each case. These values, as well as the degrees of freedom for FEM and TEPEM (for transversal order $\mathsf{p} = \{4, 6, 8, 10\}$), are displayed in Table 2. As can be seen, reduction in the average computational time is around 200 and 21 times for $\mathsf{p} = 4$ and $\mathsf{p} = 6$, respectively, compared to the typical FEM simulation. The TEPEM, considering the lower values of transversal enrichment considered here ($\mathsf{p} = 4, 6$), is capable to predict flow structure in close agreement with the FEM solution. In Figure 10, it is inspected the pressure approximation (for lower transversal orders) in two different regions in the arterial tree. Even considering discontinuous the pressure field in the TEPEM, the solution by this method has a high level of agreement in both regions when compared to the FEM solution that, reminding, is performed in a mesh employed in standard hemodynamic simulations.

Regarding the velocity field, in Figure 11 it is presented the comparison of TEPEM and FEM approximations for the same two regions studied before. It is also remarkable that, even for such complex regions, the velocity profile provided by employing a transversal order of only $\mathsf{p} = 4$ is largely in agreement to the FEM solution. As expected, the agreement increases as the transversal order is incremented. This results into a reasonably accurate approximation for velocity and pressure with a gain in the computational cost of approximately 200 times.

Table 2: Comparison of averaged computational time (in minutes) and degrees of freedom for the simulation of coronary blood flow using TEPEM and FEM. TEPEM simulations were run with NP $= 10$, while FEM simulations were run with NP $= 50$.

	FEM	TEPEM			
		$\mathsf{p} = 4$	$\mathsf{p} = 6$	$\mathsf{p} = 8$	$\mathsf{p} = 10$
Mesh DoFs	2 814 056	78 226	153 469	253 866	379 417
Time $\times$ NP	1 558.85	8.16	74.03	324.82	1003.05

6 FINAL REMARKS

The capabilities of the Transversally Enriched Pipe Element Method (TEPEM) were explored in the context of branching vascular networks. The basic idea of this methodology is supported by the discriminated utilization of axial and transversal polynomials for the physical fields, providing a severe reduction in the computational cost but keeping accuracy according to medical needs. Through numerical examples, it has been demonstrated that the TEPEM can become an extremely efficient tool in terms of the trade-off between accuracy and computational cost, delivering excellent predictions at a fraction of the effort required by standard FEM techniques.

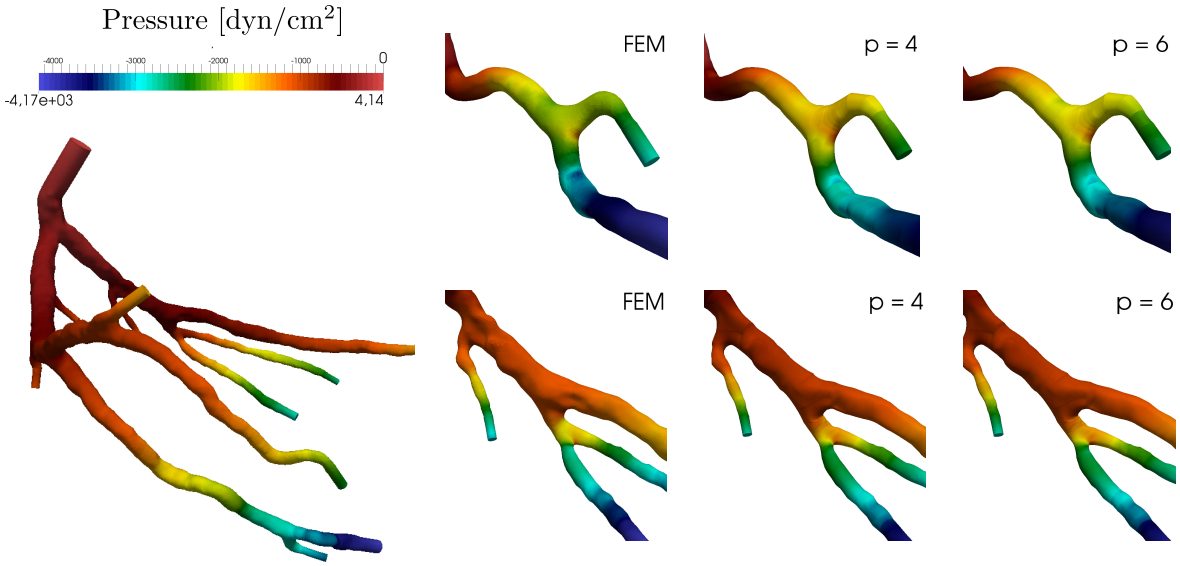

Figure 10: Comparison of pressure field between TEPEM and reference FEM solution, for different transversal polynomial orders and in two different regions of the coronary network.

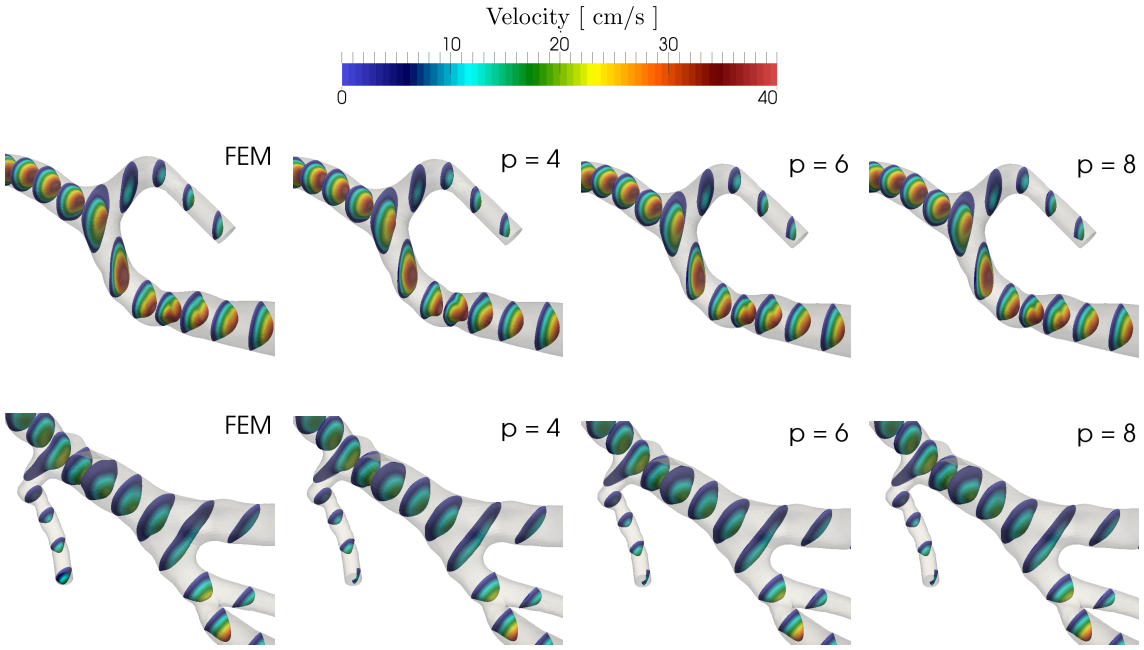

Figure 11: Comparison of velocity profiles for different approximation orders of the TEPEM and FEM in two selected regions of left arterial coronary tree.

ACKNOWLEDGEMENTS

This work was partially suported by the Brazilian agencies CNPq and FAPERJ. The support of these agencies is gratefully acknowledged.

REFERENCES

Blanco, P., Mansilla Alvarez, L., and Feijóo, R. (2015). Hybrid element-based approximation for the Navier–Stokes equations in pipe-like domains. *Comp. Meth. Appl. Mech. Engrg.*,

283:971–993.

Blanco, P., Watanabe, S., Dari, E., Passos, M., and Feijóo, R. (2014). Blood flow distribution in an anatomically detailed arterial network model: criteria and algorithm. *Biomechanics and Modeling in Mechanobiology*, 13:1303–1330.

Fox, J. and Hugh, A. (1966). Localization of atheroma: a theory based on boundary layer separation. *British Heart Journal*, 28(3):388.

Giannoglou, G., Soulis, J., Farmakis, T., Farmakis, D., and Louridas, G. (2002). Haemodynamic factors and the important role of local low static pressure in coronary wall thickening. *International journal of Cardiology*, 86(1):27–40.

Grinberg, L., Anor, T., Madsen, J., Yakhot, A., and Karniadakis, G. (2009). Large-scale simulation of the human arterial tree. *Clinical and Experimental Pharmacology and Physiology*, 36:194–205.

Grinberg, L., Cheever, E., Anor, T., Madsen, J., and Karniadakis, G. (2011). Modeling blood flow circulation in intracranial arterial networks: a comparative 3d/1d simulation study. *Ann. Biomed. Engng.*, 39(1):297–309.

Gupta, A. (1978). A finite element for transition from a fine to a coarse grid. *International Journal for Numerical Methods in Engineering*, 12(1):35–45.

Hughes, T. and Lubliner, J. (1973). On the one-dimensional theory of blood flow in the larger vessels. *Mathematical Biosciences*, 18:161–170.

Ku, D., Giddens, D., Zarins, C., and Glagov, S. (1985). Pulsatile flow and atherosclerosis in the human carotid bifurcation. Positive correlation between plaque location and low oscillating shear stress. *Arteriosclerosis*, 5:293–302.

Lucia, D., Beran, P., and Silva, W. (2004). Reduced-order modeling: new approaches for computational physics. *Prog. Aerosp. Sci.*, 40(1-2):51–117.

Mansilla Alvarez, L., Blanco, P., Bulant, C., Dari, E., Veneziani, A., and Feijóo, R. (2017). Transversally enriched pipe element method (tepem): An effective numerical approach for blood flow modeling. *Int. J. Num. Meth. Biomed. Engng.*, 33(4).

Perktold, K., Resch, M., and Peter, R. (1991). Three-dimensional numerical analysis of pulsatile flow and wall shear stress in the carotid artery bifurcation. *J. Biomech.*, 24(6):409–420.

Quarteroni, A. and Rozza, G., editors (2014). *Reduced Order Methods for Modeling and Computationtal Reduction*. Springer.

Taylor, C., Fonte, T., and Min, J. (2013). Computational fluid dynamics applied to cardiac computed tomography for noninvasive quantification of fractional flow reserve. *Journal of the American College of Cardiology*, 61(22):2233–2241.

Taylor, C. A., Hughes, T. J., and Zarins, C. K. (1998). Finite element modeling of blood flow in arteries. *Computer methods in applied mechanics and engineering*, 158(1-2):155–196.

Zarins, C., Giddens, D., Bharadvaj, B., Sottiurai, V., Mabon, R., and Glagov, S. (1983). Carotid bifurcation atherosclerosis. Quantitative correlation of plaque localization with flow velocity profiles and wall shear stress. *Circ. Res.*, 53:502–514.